PCCP

ROYAL SOCIETY OF CHEMISTRY

PAPER

View Article Online
View Journal

Cite this: DOI: 10.1039/d1cp03023j

σ–Hole activation and structural changes upon perfluorination of aryl halides: direct evidence from gas phase rotational spectroscopy†

Dingding Lv, [a] Assimo Maris, [a] Luca Evangelisti, [a] Andrea Maggio,[a] Wentao Song,[a] Ashley A. Elliott,[b] Sean A. Peebles, [b] Justin L. Neill,[c] Matt T. Muckle,[c] Brooks H. Pate, [c] Rebecca A. Peebles *[b] and Sonia Melandri *[a]

Received 2nd July 2021,
Accepted 8th August 2021

DOI: 10.1039/d1cp03023j

rsc.li/pccp

Enhancement of the σ–hole on the halogen atom of aryl halides due to perfluorination of the ring is demonstrated by use of the Extended Townes–Dailey (ETD) model coupled to a Natural Atomic Orbital Bond analysis on two perfluorinated aryl halides (C_6F_5Cl and C_6F_5Br) and their hydrogenated counterparts. The ETD analysis, which quantifies the halogen p-orbitals populations, relies on the nuclear quadrupole coupling constants which in this work are accurately determined experimentally from the rotational spectra. The rotational spectra investigated by Fourier-transform microwave spectroscopy performed in supersonic expansion are reported for the parent species of C_6F_5Cl and C_6F_5Br and their ^{13}C, ^{37}Cl or ^{81}Br substituted isotopologues observed in natural abundance. The experimentally determined rotational constants combined with theoretical data at the MP2/aug-cc-pVTZ level provide precise structural information from which an elongation of the ring along its symmetry axis due to perfluorination is proved.

Introduction

Covalently bound halogen atoms show unique properties both nucleophilic and electrophilic. It is well known that they can act as electron donors in the formation of hydrogen bonds[1] and also as electron acceptors in halogen bonds.[2,3]

While the behavior of halogen atoms as hydrogen bond acceptors is easily attributable to their rich electron cloud, their behavior as electrophilic ligands is related to a particular feature of the halogen atom (in particular Cl, Br or I) which shows a region of positive electrostatic potential on its outermost portion (called the σ–hole)[4] which can interact with another entity showing a negative electrostatic potential in the so-called σ–hole interaction. Actually, the electron density at the halogen atom shows an anisotropy which leads to the electrophilic σ–hole collinear with the C–X bond and the nucleophilic belt around the equator of X.[5–7]

Besides their intrinsic properties, when halogen atoms, in particular fluorine, act as substituents their electron withdrawing effect can dramatically change the electronic distribution in the molecules compared to the unsubstituted species. In hexafluorobenzene, for example, perfluorination causes the formation of a positive electrostatic potential region in the center of the ring. This region, differently from the one formed on the tip of the halogen atoms, is called a π–hole, because it is formed perpendicularly to the molecular frame.[8] The existence of such a hole has been demonstrated by quantum chemical calculations[9,10] but also by the direct experimental observation of a lone pair···π–hole interaction in the 1 : 1 complex of water with hexafluorobenzene[11] or pentafluoropyridine[12] by rotational spectroscopy. The rotational study on the complex pentafluoropyridine-water indicates that the presence of the fluorine substituents not only creates a different binding site (the π–hole) but also weakens the capacity of the heterocyclic nitrogen to act as a hydrogen bond acceptor. The concepts of σ- and π–hole can be extended to other classes of atoms and molecular frames and their importance in biological systems and the design of new materials has been described.[13]

On these premises, studying the effects of perfluorination on the structural and electronic properties of aryl halides seems

[a] Dipartimento di Chimica "G. Ciamician", Università di Bologna, via F. Selmi 2, 40126, Bologna, Italy. E-mail: sonia.melandri@unibo.it
[b] Department of Chemistry and Biochemistry, Eastern Illinois University, 600 Lincoln Ave., Charleston, IL 61920, USA
[c] Department of Chemistry, University of Virginia, McCormick Rd., PO Box 411319, Charlottesville, VA 22904, USA

† Electronic supplementary information (ESI) available: Experimental (r_0 and r_s) and theoretical (r_e, MP2/aug-cc-pVTZ) principal axis system coordinates (Å) of C_6F_5Cl, C_6F_5Br, C_6H_5Cl and C_6H_5Br (Tables S1–S4), measured transition frequencies of isotopologues of C_6H_5Cl and C_6H_5Br, in MHz (Tables S5 and S6), fitted structural parameters by STRFIT program for the C_6F_5Cl, C_6F_5Br, C_6H_5Cl, C_6H_5Br (Table S7), orbital population and VPPA of the p-orbitals of the halogen atom in C_6H_5X and C_6F_5X (X = Cl, Br) calculated with the ETD model and the NAO analysis (Table S8), References. See DOI: 10.1039/d1cp03023j

particularly interesting since the electronic charge distributions shown by the halogen atom in halobenzenes can be altered by substitution of fluorine atoms on the aromatic ring.

The effects of perfluorination can also be important in relation to the reactivity of aryl halides. These molecules are used as synthetic intermediates that can undergo nucleophilic aromatic substitution reactions (S_NAr) when strong electron-withdrawing groups are present on the aromatic ring. These processes have been studied in condensed phase[14] and in the gas phase.[15] Another effect of the addition of strong electron-withdrawing groups to an arene is that the aryl moiety is converted into a good leaving group and this favours the occurrence of S_N2 reactions on a halogen substituent (generally bromine or iodine).[16]

Based on these considerations chloropentafluorobenzene (C_6F_5Cl) and bromopentafluorobenzene (C_6F_5Br) are chosen as case studies to investigate the effect of perfluorination on the molecular structure and electronic properties. Rotational spectroscopy is chosen as the technique of investigation since its high resolution and sensitivity allows the accurate determination of structural parameters both in molecules[17,18] and non-covalently bound complexes.[19,20] Moreover, rotational transitions can show hyperfine splittings due to the coupling of the nuclear spin *via* its quadrupole moment (if the nucleus has spin greater than 1/2) to the overall rotation. Analysis of the nuclear hyperfine structure of the rotational spectra allows the accurate determination of the nuclear coupling tensor or its main components.

Regarding the latter, the Townes–Dailey (TD)[21] model has been used for decades to interpret the nuclear coupling constants in terms of p valence orbital's populations and recently its three dimensional formulation, the Extended Townes-Dailey (ETD) method, has been proposed.[22] The results provide insight into the electronic properties of the bonds involving the quadrupole bearing atom: orbital hybridization, degree of covalence in a chemical bond (or ionic bond character), molecular geometry and recently to discuss the potential of molecules in forming a halogen bond.[23,24] In a recent theoretical paper it has been proposed to use a modified ETD model to calculate the Valence p-orbital Population Anisotropy (VPPA) directly related to the quadrupole coupling tensor to quantify and visualize those properties.[25] The VPPA, being related to charge imbalance, also allows the quantification of other properties such as the extent of the σ–hole on the halogen atoms.

The interest in the structure and electronic properties of halobenzenes and poly and perfluorinated arenes is proven by the rotational spectroscopy studies performed on several species: fluorobenzene,[26,27] 1,2- and 1,3-difluorobenzene,[28] 1,2,3-trifluorobenzene,[29] 1,2,4-trifluorobenzene,[30] 1,2,3,4-tetrafluorobenzene,[31] pentafluorobenzene,[32] chlorobenzene,[33] bromobenzene,[34,35] iodobenzene,[36,37] 1-chloro-2-fluorobenzene,[38] 1-chloro-3-fluorobenzene,[39] 1-chloro-4-fluorobenzene.[40]

C_6F_5Cl and C_6F_5Br are important fine chemical intermediates and have broad application prospects in the fields of medicine, pesticides, liquid crystals and olefin polymerization catalysis.[41] Their r_α structures were investigated by Haloui A. and Haloui E.[42,43] utilizing NMR spectroscopy. As stated by the authors, the accuracy of that technique is significantly less than that of microwave spectroscopy and solvent effect cannot be neglected.

On the contrary, the precise data obtained by rotational spectroscopy for the perfluorinated aryl halides can be compared to those of the non-perfluorinated compounds in trying to assess the effects of successive addition of fluorine atoms on the molecular properties in isolated conditions. They can also be used to benchmark quantum chemical results from widely used computational methods to assess their performance in modelling structural and electronic properties.

In the previously cited work by Rinald and Wu[25] the VPPA method is applied to theoretically calculated values of the quadrupole tensors and orbital populations but we propose to use it here to derive those electronic properties directly from the experimentally determined quadrupole coupling tensor in order to gain insight into the electronic properties of the C–X (X = Cl, Br) bond and their changes upon perfluorination.

Results and discussion

Theoretical

The *ab initio* full optimizations of the structures of the perfluorinated compounds C_6F_5Cl and C_6F_5Br and their hydrogenated counterparts C_6H_5Cl and C_6H_5Br were carried out with the GAUSSIAN 16 suite of programs[44] using second-order Møller−Plesset (MP2) theory at the aug-cc-pVTZ level under the constraint of C_{2v} symmetry. This method has proved its reliability in calculating rotational constants with good accuracy.[45] The principal axes system's coordinates of the optimized structures are available in the ESI† (Tables S1–S4). The quadrupole coupling constants were estimated from the MP2/aug-cc-pVTZ optimized structures using the Douglas–Kroll–Hess 2nd order scalar relativistic core Hamiltonian,[46] in the point nuclear approximation, with the recontracted aug-cc-pVTZ-DK basis set[47,48] freely available at Basis Set Exchange Database.[49]

The rotational spectra were predicted based on the theoretical values of the spectroscopic constants for the most abundant isotopologue which are reported in Table 1.

Due to the C_{2v} molecular symmetry only a-type transition lines can be observed. Also, considering the natural relative abundance of the two most abundant isotopes of chlorine (^{35}Cl 76% and ^{37}Cl 24%), the intensity of the rotational spectra belonging to ^{37}Cl isotopes is expected to be 1/3 of that for the ^{35}Cl species. Bromine has two almost equally abundant isotopes (^{79}Br 50.7% and ^{81}Br 49.3%), thus the rotational spectra of the two isotopologues should have very similar intensity. Regarding ^{13}C, considering the natural abundance and the C_{2v} symmetry of the molecules, four mono-substituted species are expected (see Fig. 1 for numbering of the atoms), two with 1.1% abundance (^{13}C1, ^{13}C4) and two with 2.2% (^{13}C2,^{13}C3) abundance with respect to the parent species. Due to the nuclear quadrupole coupling of both isotopes of chlorine and bromine

Table 1 *Ab initio* (MP2/aug-cc-pVTZ) rotational constants (*A*, *B*, *C*), quadrupole coupling constants (χ_{aa}, χ_{bb}, χ_{cc}), asymmetry parameter (η), planar moments of inertia (M_{aa}, M_{bb}) and electric dipole moment (μ_a) of parent species

	C_6F_5Cl	C_6F_5Br	C_6H_5Cl	C_6H_5Br
A (MHz)	1027.83	1027.69	5693.27	5691.00
B (MHz)	751.91	496.97	1578.01	1000.35
C (MHz)	434.24	334.98	1235.55	850.80
χ_{aa} (MHz)	−80.85	653.80	−71.62	562.16
χ_{bb} (MHz)	43.64	−353.16	37.57	−292.37
χ_{cc} (MHz)	37.20	−300.65	34.05	−269.80
η (MHz)[a]	−0.0870	−0.0928	−0.0597	−0.0505
M_{aa} (u Å^2)[b]	672.13	1016.93	320.26	505.20
M_{bb} (u Å^2)	491.69	491.76	88.77	88.80
μ_a (D)	−0.37	−0.56	1.70	1.72

[a] η is the asymmetry parameter defined as $\eta = (\chi_{bb} - \chi_{cc})/\chi_{aa}$. [b] The planar moments of inertia: $M_{aa} = \sum_i m_i a_i^2$, $M_{bb} = \sum_i m_i b_i^2$, M_{cc} is zero by symmetry.

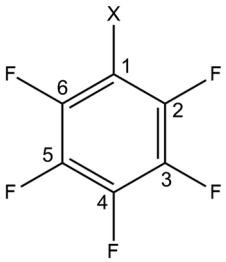

Fig. 1 The atom numbering scheme used to describe the structural parameters (X = Cl, Br).

and their nuclear spin quantum number $I = 3/2$, the rotational spectrum of C_6F_5Cl and C_6F_5Br is expected to be split into a multiplet of hyperfine components.

Microwave spectra

For C_6F_5Cl, initial predictions at the MP2/aug-cc-pVTZ level were accurate enough to quickly identify a-type $K_a = 0$ and 1 transitions close to predicted frequencies and with hyperfine patterns in agreement to the *ab initio* ones. Unresolved and partially overlapping hyperfine components meant some strong transitions had to be excluded from the fit; however, 217 hyperfine components were fitted for ^{35}Cl, and 87 were fitted for ^{37}Cl. Using the SPFIT package[50] the spectra were fitted by a reduced semirigid Hamiltonian in the I^r representation which includes an additional term to fit the nuclear hyperfine structure.[51] Only D_J and d_1 centrifugal distortion constants were determined, and these were fixed to the values from the ^{35}Cl isotopologue for analyses of all other isotopic species.

Initial assignments of ^{13}C spectra for the ^{35}Cl isotopologue were made using a reduced bandwidth spectrum with a high number of experimental averages, to enhance the signal-to-noise ratio (see Experimental section). Spectra of all four unique ^{13}C species were assigned, with 45 and 36 transitions fitted for the 2% abundance species (^{13}C2 and ^{13}C3, respectively), and 31 and 33 transitions fitted for the 1% abundance species (^{13}C1 and ^{13}C4, respectively). Nuclear quadrupole

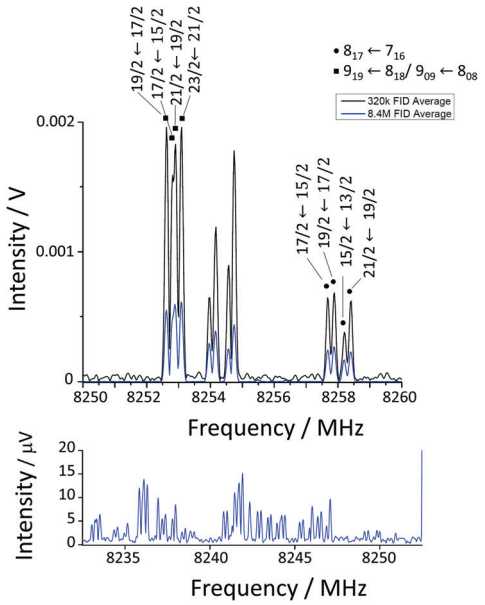

Fig. 2 Top: Hyperfine components $F' \leftarrow F''$ for the $8_{1,7} \leftarrow 7_{1,6}$, $8_{2,7} \leftarrow 7_{2,6}$ (unlabeled in the figure), $9_{1,9} \leftarrow 8_{1,8}$ and $9_{0,9} \leftarrow 8_{0,8}$ transitions of C_6F_5Cl parent species. Bottom: 1000× vertical magnification showing detail of the same transitions (overlapping) for all four ^{13}C species.

coupling constants for ^{35}Cl were adjusted for all ^{13}C species, giving values identical to the parent to within experimental uncertainties. Note that only the diagonal terms of the nuclear quadrupole coupling tensor are different from zero due to the symmetry of the molecules. Full lists of assigned transitions for all isotopic species can be found in Table S5 (ESI†), while Fig. 2 shows resolved and unresolved hyperfine components for several transitions of the parent and ^{13}C isotopologues.

For C_6F_5Br, a total of 224 lines were included in the fit for ^{79}Br and 243 lines for ^{81}Br, and as for the previous system, all transitions were fitted with the SPFIT program[50] to a semirigid Hamiltonian in the I^r representation including nuclear quadrupole coupling terms.[51]

The rotational spectra of the two ^{13}C most abundant species were also measured, corresponding to the ^{13}C substitution at C2 and C3 in the isotopologue bearing ^{79}Br. The observation of these isotopologues' spectra was close to the limit of detection thus the spectra originating from substitution of atoms C1 and C4 could not be observed. In total, 18 lines were observed for the ^{13}C2 and 11 lines for the ^{13}C3 species. Due to the small number of observable lines, the values of the quadrupole coupling constants were fixed to those of the parent species in the fit.

Full lists of the transition frequencies for the parent and isotopologues species (^{81}Br, ^{13}C2 and ^{13}C3) are available from Table S6 (ESI†). The hyperfine structures of the $12_{0,12} \leftarrow 11_{0,11}$ and $12_{1,12} \leftarrow 11_{1,11}$ transitions of C_6F_5Br are depicted in Fig. 3. The rotational constants and nuclear quadrupole coupling constants of all the observed species are summarized in Tables 2 and 3 for C_6F_5Cl and C_6F_5Br, respectively.

In agreement with the prediction of a planarity, the planar moments of inertia along the *c* axis ($M_{cc} = \Sigma_i m_i c_i^2$) are very close

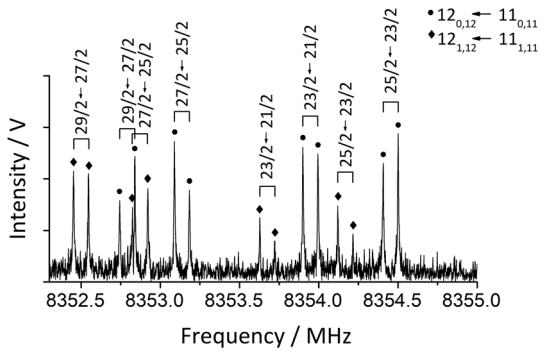

Fig. 3 The $12_{0,12} \leftarrow 11_{0,11}$ and $12_{1,12} \leftarrow 11_{1,11}$ transitions of the C_6F_5Br parent species showing the main $F' \leftarrow F''$ hyperfine components.

Table 3 Experimental spectroscopic parameters of parent and three observed isotopologues of C_6F_5Br

	Parent	^{81}Br	^{13}C2=	^{13}C3=
A (MHz)	1027.7040(2)[a]	1027.7040(2)	1024.743(6)	1024.725(8)
B (MHz)	495.05251(4)	489.42319(4)	495.056(2)	493.925(3)
C (MHz)	334.11342(2)	331.53944(2)	333.8016(1)	333.2851(1)
χ_{aa} (MHz)	637.68(3)	532.83(3)	[637.68][b]	[637.68]
χ_{bb} (MHz)	−346.12(4)	−289.2(2)	[−346.12]	[−346.12]
χ_{cc} (MHz)	−291.56(4)	−243.6(2)	[−291.56]	[−291.56]
η (MHz)[c]	−0.0856(1)	−0.086(1)	—	—
N[d]	224	243	18	11
M_{aa} (u Å^2)[e]	1020.8507(1)	1032.5933(1)	1020.843(4)	1023.181(5)
M_{bb} (u Å^2)	491.7466(1)	491.7474(1)	493.167(4)	493.176(5)
M_{cc} (u Å^2)	0.0088(1)	0.0081(1)	0.009(4)	0.009(5)
$\Delta\nu_{rms}$(kHz)[f]	13.9	5.9	2.7	2.4

[a] Error in parentheses in units of the last digit. [b] Fixed at the ^{79}Br monomer value. [c] η is the asymmetry parameter, defined as $\eta = (\chi_{bb} - \chi_{cc})/\chi_{aa}$. [d] N = Number of transitions fitted. [e] The planar moments of inertia $M_{gg} = \Sigma_i m_i g_i^2$ ($g = a, b, c$). [f] $\Delta\nu_{rms} = [\Sigma(\nu_{obs} - \nu_{calc})^2/N]^{1/2}$.

to zero. The slightly positive values are consistent with low-frequency, small amplitude out-of-plane vibrations, which would be expected for rigid ring molecule.[34]

Structural considerations

For the determination of the structures, we relied on the information carried by the rotational spectra of the isotopologues combined with that obtained by the theoretical calculations. From the isotopologues' experimental rotational constants, it is possible to determine the principal axis coordinates of the substituted atoms (substitution coordinates, r_s) using Kraitchman's single isotopic substitution analysis.[52] The obtained values are reported in the ESI† (Tables S1–S4) for the two perfluorinated systems (C_6F_5Cl and C_6F_5Br) and their hydrogenated counterparts (the rotational constants for C_6H_5Cl and C_6H_5Br were taken from ref. 33 and 34 respectively) where they are also compared to the r_e values determined by the theoretical calculations. Since the atom coordinates in Kraitchman's equations appear as their squares, their signs cannot be unambiguously determined but must be compared to the calculate ones. Costain's rule was used to calculate the uncertainties.[53]

As a second method we utilized the *ab initio* structure as a starting point and adjusted the ring structural parameters and the position of the Cl or Br atom to obtain the best fit to the set of planar moments of inertia measured for the isotopologues of each molecular species. The fit was obtained using the STRFIT program[54] and the resulting structure adjusted to reproduce the vibrational ground state rotational parameters is known as the r_0 structure.

In the fitting procedure we imposed the C_{2v} symmetry by adjusting the C–C bonds and angles in matching couples and pinning the halogen atom (X), C1 and C4 atoms onto the symmetry axis. A suitable fitting was possible adjusting the C1–X, C1–C2 and C2–C3 (and their corresponding C1–C6 and C5–C6) bond lengths, the C2C1X and C3C2C1 (and their corresponding C6C1X and C5C6C1) angles and the C4–C1 distance. Only in the case of C_6F_5Br this last value was fixed to a corrected *ab initio* value. The correction was obtained accounting for the difference between the fitted distance and the theoretical one in C_6H_5Br. The results of the fitting procedures are reported in the ESI† (Table S7) while the theoretical and experimental structures are depicted in Fig. 4.

Examination of the structures allows us to make some considerations and comparisons between chlorine and bromine substituted molecules as well as hydrogenated and

Table 2 Experimental spectroscopic parameters of parent and five observed isotopologues of C_6F_5Cl

	Parent	^{37}Cl	^{13}C1	^{13}C2	^{13}C3	^{13}C4
A (MHz)	1028.5412(2)[a]	1028.5439(7)	1028.568(2)	1025.572(2)	1025.563(2)	1028.578(2)
B (MHz)	751.8207(2)	734.4795(2)	750.4372(4)	751.6505(4)	750.7696(4)	748.7217(4)
C (MHz)[b]	434.3531(3)	428.5081(2)	433.898(5)	433.7654(4)	433.4701(4)	433.3233(4)
χ_{aa} (MHz)	−79.52(2)	−62.67(2)	−79.7(5)	−79.45(5)	−79.43(5)	−79.51(7)
χ_{bb} (MHz)	43.6(1)	34.39(1)	43.7(2)	43.56(3)	43.60(3)	43.59(3)
χ_{cc} (MHz)	35.92(2)	28.27(4)	36.0(3)	35.89(9)	35.84(9)	35.91(9)
η (MHz)[c]	−0.0965(4)	−0.098(2)	−0.096(9)	−0.0967(9)	−0.098(2)	−0.097(2)
N[d]	217	87	31	45	36	33
M_{aa} (u Å^2)[e]	672.1865(5)	688.0580(5)	673.4227(7)	672.340(1)	673.129(1)	674.970(1)
M_{bb} (u Å^2)	491.3348(5)	491.3341(5)	491.3189(7)	492.758(1)	492.763(1)	491.317(1)
M_{cc} (u Å^2)	0.0204(5)	0.0198(5)	0.0235(7)	0.020(1)	0.019(1)	0.020(1)
$\Delta\nu_{rms}$ (kHz)[f]	6.1	4.8	5.5	4.9	4.1	5.0

[a] Error in parentheses in units of the last digit. [b] Centrifugal distortion constants were adjusted for the parent species and fixed at those values for all other species: D_J = 3.8(1.0) Hz, d_1 = 3.4(9) Hz. [c] η is the asymmetry parameter, defined as $\eta = (\chi_{bb} - \chi_{cc})/\chi_{aa}$. [d] N = Number of transitions fitted. [e] The planar moments of inertia $M_{gg} = \Sigma_i m_i g_i^2$ ($g = a, b, c$). [f] $\Delta\nu_{rms} = [\Sigma(\nu_{obs} - \nu_{calc})^2/N]^{1/2}$.

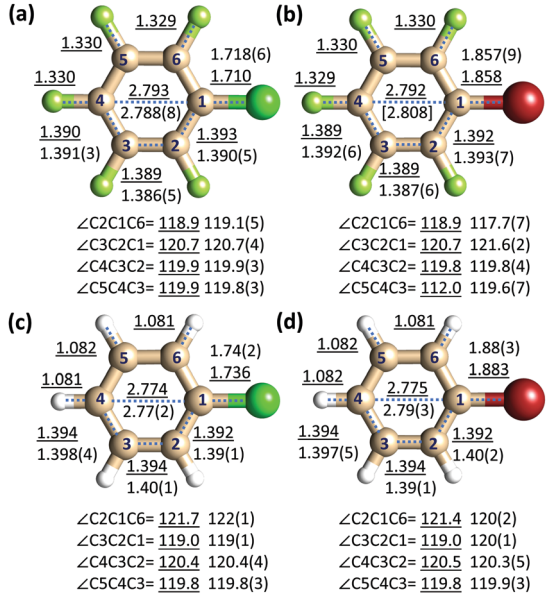

Fig. 4 Geometries of (a) C_6F_5Cl, (b) C_6F_5Br, (c) C_6H_5Cl and (d) C_6H_5Br; MP2/aug-cc-pVTZ parameters (underlined values) and experimental values (normal font). Distances in Å, angles in degrees. The R(C1C4) parameter in C_6F_5Br (in square brackets) is fixed to 2.808 Å (see text for details). Error in parentheses in units of the last digit. Rotational constants of C_6H_5Cl and C_6H_5Br taken from ref. 33 and 34 respectively.

perfluorinated species. Let us first consider the structural changes occurring when chlorine is substituted by bromine. We observe an increase of 0.14(1) Å in the C–X bond length both in the hydrogenated and perfluorinated species in agreement with difference in their covalent radii (R_{Br}–R_{Cl} = 0.15 Å) while the C–C bond lengths do not change significantly. As regards the ring angles, the biggest changes are seen in the *ipso* and *ortho* angles with an average change of −1.4° and 0.8° respectively while the other angles show smaller differences. These effects on the angles are not very large and fall close to the uncertainties with which they are determined thus they should be considered an indication of a trend more than accurate values. Focusing alternatively on the chlorine or the bromine substituted molecules we can infer the effects of perfluorination on the structural properties. In this case the bond lengths are not affected very much but we can see larger changes on the angles. Upon perfluorination of the ring, the *ipso* angles show an average decrease of 2.6° and the *ortho* angles an average increase of 1.9° while the *meta* and *para* angles decrease by less than 1°.

A more direct evaluation of structural changes can be done directly using the coordinates of the substituted atoms (r_s). In this way we calculated the C2–C6 distance and C3–C5 distance in C_6F_5X (X = H, F, Cl, Br) which are compared to the same parameters of C_6H_5X (X = H, F, Cl, Br) in Table 4. In the same table the *ab initio* values (r_e) are also reported.

The observed geometric changes of the C2–C6 distance and C3–C5 distance in C_6F_5X relative to C_6H_5X are significant and consistent. The C2–C6 and C3–C5 distances are shorter in the perfluorinated molecules than those in the hydrogenated ones.

Table 4 *Ab initio* structural parameters (r_e, MP2/aug-cc-pVTZ) and parameters derived from substitution structure (r_s) for the C_6H_5X and C_6F_5X (X = H, F, Cl, Br)

	C2C6 (Å)		C3C5 (Å)	
	r_s	r_e	r_s	r_e
C_6H_6	—	2.4151	—	2.4151
C_6H_5F[27]	2.434(4)[a]	2.4307	2.416(4)	2.4131
C_6H_5Cl[33]	2.430(6)	2.4274	2.422(6)	2.4069
C_6H_5Br[34]	2.426(6)	2.4281	2.412(8)	2.4110
C_6F_5H[32]	2.373(3)	2.3831	2.404(3)	2.4140
C_6F_6	—	2.4077	—	2.4077
C_6F_5Cl	2.3884(8)	2.3998	2.3972(8)	2.4069
C_6F_5Br	2.384(4)	2.3974	2.398(4)	2.4065

[a] Error in parentheses in units of the last digit.

In addition, the changes in the C2–C6 distances are greater than those of the C3–C5 distances. In C_6F_5Cl (or C_6F_5Br), the C2–C6 distance is 0.01 Å (or 0.032 Å) shorter than in C_6H_5Cl (or C_6H_5Br), while the C3–C5 distance is slightly shorter, but not outside the error limits. These results, which have been calculated independently of the structural fit, are in agreement with the latter and in particular with the reduction of the *ipso* and *para* angles upon fluorination as they are in agreement also with the theoretical distances reported in the table. These observed geometric changes also agree with the trends found in C_6F_5H[32] relative to C_6H_6 and in C_6F_6 relative to C_6H_5F.[27]

Electronic effects

According to the ETD model, only the valence electron population in the p-orbitals contribute to the quadrupole coupling tensor. If the atomic quadrupole tensor axes system and the p-orbitals are coincident, the populations (P) and the nuclear quadrupole coupling constants (χ) are related by three simple equations which contain the population of each orbital and the one-electron contribution to the coupling tensor, χ_0:[22]

$$\chi_{xx} = \chi_0\left(P_{xx} - \frac{1}{2}P_{yy} - \frac{1}{2}P_{zz}\right) \quad (1)$$

$$\chi_{yy} = \chi_0\left(-\frac{1}{2}P_{xx} + P_{yy} - \frac{1}{2}P_{zz}\right) \quad (2)$$

$$\chi_{zz} = \chi_0\left(-\frac{1}{2}P_{xx} - \frac{1}{2}P_{yy} + P_{zz}\right) \quad (3)$$

The experimentally derived χ_0 value for ^{79}Br is −769.756 MHz while for ^{35}Cl this value is 109.746 MHz.[55]

From the rotational transitions the components of the nuclear quadrupolar tensor in the principal system of inertia of the molecule (a, b and c) are derived and according to the symmetry of the molecules examined in this paper, the principal inertial axes are coincident with the orientation of the p-orbitals of the halogen atom. In fact, the a axis (z axis) lies along the C–X bond, b is in the plane of the molecule (y axis) and c axis (x axis) perpendicular to the molecular plane. Since the inertial principal axes orientation coincides with that of the principal axes of the quadrupolar nucleus, the determination of

the population along the natural axes (P_{xx}, P_{yy}, P_{zz}) is straightforward through the previously introduced equations (eqn (1)–(3)) where $\chi_{zz} = \chi_{aa}$, $\chi_{yy} = \chi_{bb}$ and $\chi_{xx} = \chi_{cc}$.

One complication arises from the three equations not being linearly independent and some physical assumptions must be put in place to solve the system. The assumption used in the original TD model is that the electronic population of the p-orbital in the plane of the molecule and perpendicular to the C–X bond (P_{yy}) is equal to 2 and the populations of the other p-orbitals (P_{xx} and P_{yy}) are also expected to be very close to 2. With these assumptions the populations of the p-orbitals of the chlorine and bromine atoms were estimated from the experimental quadrupole coupling constants for the hydrogenated and perfluorinated benzene halides (ESI,† Table S8). In the modified ETD model presented in ref. 25 the suggestion is to use the p-population anisotropies (calculated as differences in orbital's population along the axes with respect to the average population, ΔP_{xx}, ΔP_{yy} and ΔP_{zz}) in order to quantify the electronic properties. Those values are reported in the ESI† (Table S8) and summarized in Fig. 5.

For comparison and to gain a more complete picture of the valence orbitals, a Natural Atomic Orbital (NAO) analysis was performed with the Natural Bond Orbital (NBO)[56] package within the Gaussian 16 suite of programs to calculate the populations in the halogen's valence p-orbitals. The NAO populations and the VPPA values derived from them are also reported in the ESI† (Table S8) and in Fig. 5 for comparison with the ones determined using the ETD model.

The NAO populations are also used to characterize the lone pair halogen's orbitals (indicated as LP in Fig. 5). In all four molecular systems the three lone pairs of the halogen atom are very similar. The C–X bond is formed by a sp hybrid orbital with essentially s character. In Fig. 5 this is indicated by the exponent to the sp label which reports the ratio between p and s fraction of population in the orbital. The other lone pairs are in two p orbitals perpendicular to the C–X bond. Looking at the VPPA values and the orbital's labels we can see that the orbital directed along the z axis shows a decrease in population with respect to the average (ΔP_{zz} negative) while the other two show an excess (ΔP_{xx} and ΔP_{yy} positive). As discussed in ref. 25 the negative value of ΔP_{zz} is a direct measure of the strong electron density deficiency along the C–X bond which is also known as the σ–hole but we can also add that the p populations in the other two orbitals are related to the electron rich equatorial belt around the halogen atom.

Looking at the ΔP_{zz} values for the four molecules we can see that this deficiency not only increases in going from chlorine to bromine, as it has been extensively pointed out in the literature, but it also increases upon ring perfluorination in the systems with the same X atom. In general, the effect of perfluorination is to diminish the overall p population on the halogen atom both increasing the σ–hole and decreasing the nucleophilic equatorial belt.

A visualization of these effects can be obtained from the depiction of the molecular electrostatic potentials (ESP) shown in Fig. 6. In this picture we can see the molecules along an axis perpendicular to the molecular plane while the smaller pictures are the side views along the direction of the C–X bond.

The regions of the σ-system and Br or Cl atom that become positively charged and create the σ- or π–hole are seen as blue regions at the center of the ring and at the tip of Cl or Br, respectively. As discussed in the introduction, the σ–hole can generate the halogen bond located along the direction of the C–Br bond,[5,6] while the π–hole can form the lone pair···π–hole interaction located perpendicularly to the plane of aromatic ring.[11,13] In Fig. 6 we can observe that the π–hole is formed only in the perfluorinated systems and it is slightly more positive in C_6F_5Cl than in C_6F_5Br. However, the σ–hole it is present in all systems, greater in Br than in Cl while it is definitely more positive in the perfluorinated systems. A nucleophilic belt is clearly visible as an electron rich region (red) along the equator

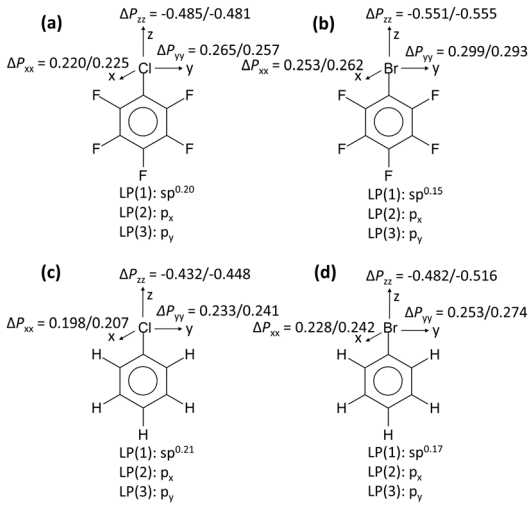

Fig. 5 VPPA values (first value from EDT, second value from NAO) and electron lone pairs (from NAO) in (a) C_6F_5Cl, (b) C_6F_5Br, (c) C_6H_5Cl and (d) C_6H_5Br.

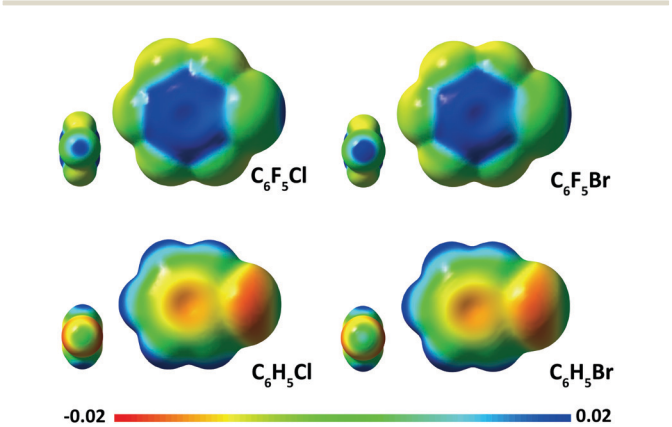

Fig. 6 Electrostatic potential maps of C_6F_5Cl, C_6F_5Br, C_6H_5Cl, and C_6H_5Br, estimated at 0.0004 a.u electron density by MP2/aug-cc-pVTZ calculations. The blue shading is the maximum (positive) potential (2.0 a.u.), and red shading is the minimum (negative) potential (−2.0 a.u). Molecules are shown along an axis perpendicular to the molecular plane; smaller pictures are the side views along the direction of the C–X bond.

of the halogen atom in the hydrogenated systems while it becomes less negative (green) in the perfluorinated ones.

Experimental

C_6F_5Cl was purchased from Sigma-Aldrich and used without further purification. A sample containing about 0.1% C_6F_5Cl in neon, at a backing pressure of around 1 atmosphere was expanded through three pulsed valves of the spectrometer, which were oriented perpendicular to the axis of microwave propagation. The spectrum was recorded using a chirped pulse (CP)-FTMW spectrometer at the University of Virginia.[57] A survey scan was recorded over the 6.0–18.0 GHz range, with ten free induction decays (FID) recorded per gas pulse. A total of 320 000 FIDs were averaged to give the final spectrum. A second spectrum was obtained over the 6.8–9.0 GHz range. The reduced bandwidth combined with a lower digitization rate allowed fifty FIDs to be averaged per gas pulse, and 8.4 million FIDs were averaged to give the final spectrum. This reduced-bandwidth, high S/N spectrum was used for observation of ^{13}C isotopologue transitions in natural abundance, as demonstrated in the inset of Fig. 2.

C_6F_5Br was purchased from Alpha Aesar (purity > 99%) and used without further purification. A COBRA-type pulsed supersonic-jet Fourier-transform microwave (FTMW) spectrometer[58–61] at the University of Bologna was used to measure the spectra. Helium at a stagnation pressure of about 2 bar, was flowed over the samples resulting in about 1% mixture of C_6F_5Br. The molecular gas was then expanded through a solenoid valve (General Valve, Series 9, nozzle diameter of 0.5 mm) into a Fabry–Perot cavity. During the expansion, the molecule can reach quite low rotational temperatures (a few K) obtaining a simplification of the spectrum with respect to room temperature spectra by depopulation of high-J and enhanced intensity for low-J transitions.

Conclusions

In this work we discuss the effects of perfluorination on the structural and the electronic properties of C_6F_5Cl and C_6F_5Br. From the rotational constants determined for several isotopologues, partial structures have been determined for the two molecules and their hydrogenated counterparts. The isotopic substitution results suggest a shortening of the distances of equivalent carbon atoms for both pairs (C2–C6 and C3–C5) of about 40 mÅ which, with the C1–C4 distant not being affected, indicates an elongation of the ring along its symmetry axis, in agreement with what has been reported in the NMR study by Haloui and Haloui,[42,43] although in that case the evidence is merely a quantum theoretical prediction.

An insight into the electronic properties of the chlorine and bromine atoms has been gained from the experimental nuclear quadrupole coupling constants determined from the rotational spectra. By applying the ETD model, the populations of the p-orbitals of the Cl and Br atoms have been derived and from those the valence p-population anisotropies (VPPA). The experimentally determined values are in agreement with those obtained using the NAO analysis and the electrostatic potential calculated at the MP2/aug-cc-pVTZ theory level. The values of the population anisotropies along the C–Cl and C–Br bonds can indicate the extent of the σ–hole present at the tip of the halogen atom while the decrease of population along the other two directions can be interpreted as a decrease of the nucleophilic belt along the equator of the halogen atom.

The results confirm that in general the σ–hole found in Br is greater than that in Cl. The results also show that the σ–hole increases upon fluorination and the chorine atom in the perfluorinated moiety acquires a similar value to that of bromine in the hydrogenated system.

These results should be helpful in the rational design and understanding of molecular systems which exploit σ–hole and π–hole interactions.

Author contributions

D. Lv: data curation, formal analysis, investigation, methodology; writing – original draft, writing – review and editing, visualization. A. Maris: conceptualization, formal analysis, investigation, methodology, validation, supervision, writing – original draft, writing – review and editing, funding acquisition; L. Evangelisti: conceptualization; formal analysis, investigation, validation, writing – review and editing; W. Song: data curation, formal analysis, investigation, methodology; writing – review and editing, A. Maggio: data curation, formal analysis, investigation, methodology; A. A. Elliott: data curation, formal analysis, investigation, methodology; S. A. Peebles: conceptualization, formal analysis, investigation, validation, supervision, resources, funding acquisition; J. L. Neill: data curation, formal analysis, investigation, methodology; writing – review and editing; M. T. Muckle: data curation, formal analysis, investigation, methodology; B. H. Pate: conceptualization, formal analysis, investigation, validation; supervision, resources, funding acquisition; R. A. Peebles: conceptualization, formal analysis, investigation, resources, validation, supervision, writing-original draft, writing – review and editing, funding acquisition; S. Melandri: conceptualization, investigation, validation, funding acquisition, resources, supervision, visualization, writing-original draft, writing – review and editing.

Conflicts of interest

There are no conflicts to declare.

Acknowledgements

We acknowledge the CINECA award under the ISCRA initiative, for the availability of high-performance computing resources and support. D. L. and W. S. thank the China Scholarship Council (CSC) for financial support. This work was supported by the Italian MIUR (Attività Base di Ricerca) and the University of Bologna (Ricerca Fondamentale Orientata). This work was

also supported by National Science Foundation grants NSF RUI-0809387 and RUI-1664900 (Eastern Illinois University) and CRIF: ID CHE-0618755 (University of Virginia).

Notes and references

1 K. Brendel, H. Mäder, Y. Xu and W. Jäger, *J. Mol. Spectrosc.*, 2011, **268**, 47–52.
2 K. A. Mason, A. C. Pearcy, I. K. Attah, S. P. Platt, S. G. Aziz and M. S. El-Shall, *Phys. Chem. Chem. Phys.*, 2017, **19**, 18603–18611.
3 A. C. Legon, *Phys. Chem. Chem. Phys.*, 2010, **12**, 7736–7747.
4 P. Politzer, P. Lane, M. C. Concha, Y. Ma and J. S. Murray, *J. Mol. Model.*, 2007, **13**, 305–311.
5 P. Politzer, J. S. Murray and T. Clark, *Phys. Chem. Chem. Phys.*, 2010, **12**, 7748–7757.
6 J. S. Murray, P. Lane, T. Clark, K. E. Riley and P. Politzer, *J. Mol. Model.*, 2012, **18**, 541–548.
7 T. Clark, M. Hennemann, J. S. Murray and P. Politzer, *J. Mol. Model.*, 2007, **13**, 291–296.
8 H. Wang, W. Wang and W. J. Jin, *Chem. Rev.*, 2016, **116**, 5072–5104.
9 D. Quiñonero, C. Garau, C. Rotger, A. Frontera, P. Ballester, A. Costa and P. M. Deyà, *Angew. Chem.*, 2002, **114**, 3539–3542.
10 I. Alkorta, I. Rozas and J. Elguero, *J. Am. Chem. Soc.*, 2002, **124**, 8593–8598.
11 L. Evangelisti, K. Brendel, H. Mäder, W. Caminati and S. Melandri, *Angew. Chem.*, 2017, **129**, 13887–13891.
12 C. Calabrese, Q. Gou, A. Maris, W. Caminati and S. Melandri, *J. Phys. Chem. Lett.*, 2016, **7**, 1513–1517.
13 A. Bauzá, T. J. Mooibroek and A. Frontera, *ChemPhysChem*, 2015, **16**, 2496–2517.
14 E. Buncel, J. M. Dust and F. Terrier, *Chem. Rev.*, 1995, **95**, 2261–2280.
15 S. Gronert, *Chem. Rev.*, 2001, **101**, 329–360.
16 L. L. Soukup and S. Gronert, *Int. J. Mass Spectrom.*, 2015, **378**, 31–37.
17 R. Sanchez, B. M. Giuliano, S. Melandri, L. B. Favero and W. Caminati, *J. Am. Chem. Soc.*, 2007, **129**, 6287–6290.
18 W. Li, A. Vigorito, C. Calabrese, L. Evangelisti, L. B. Favero, A. Maris and S. Melandri, *J. Mol. Spectrosc.*, 2017, **337**, 3–8.
19 C. Calabrese, W. Li, G. Prampolini, L. Evangelisti, I. Uriarte, I. Cacelli, S. Melandri and E. J. Cocinero, *Angew. Chem., Int. Ed.*, 2019, **58**, 8437–8442.
20 B. Velino, S. Melandri and W. Caminati, *J. Phys. Chem. A*, 2004, **108**, 4224–4227.
21 C. H. Townes and B. P. Dailey, *J. Chem. Phys.*, 1949, **17**, 782–796.
22 S. E. Novick, *J. Mol. Spectrosc.*, 2011, **267**, 13–18.
23 G. A. Cooper, C. J. Anderson, C. Medcraft and N. R. Walker, *J. Mol. Spectrosc.*, 2018, **354**, 15–23.
24 G. A. Cooper, C. Medcraft, J. D. Littlefair, T. J. Penfold and N. R. Walker, *J. Chem. Phys.*, 2017, **147**, 214303.
25 A. Rinald and G. Wu, *J. Phys. Chem. A*, 2020, **124**, 1176–1186.
26 Z. Kisiel, E. Białkowska-Jaworska and L. Pszczółkowski, *J. Mol. Spectrosc.*, 2005, **232**, 47–54.
27 L. Nygaard, I. Bojesen, T. Pedersen and J. Rastrup-Andersen, *J. Mol. Struct.*, 1968, **2**, 209–215.
28 L. Nygaard, E. R. Hansen, R. L. Hansen, J. Rastrup-Andersen and G. O. Sørensen, *Spectrochim. Acta, Part A*, 1967, **23**, 2813–2819.
29 U. Wolschendorf, U. Kretschmer and D. H. Sutter, *Zeitschrift für Naturforsch. A*, 1996, **51**, 46–52.
30 E. Jochims, H. Mäder and W. Stahl, *J. Mol. Spectrosc.*, 1996, **180**, 116–120.
31 A. Kraśnicki, M. Kr\keglewski and H. Mäder, *J. Mol. Struct.*, 2008, **882**, 123–127.
32 B. J. Bills, D. M. Carroll, A. A. Elliott, D. A. Obenchain, S. A. Peebles and R. A. Peebles, *J. Mol. Struct.*, 2012, **1023**, 149–153.
33 S. Cradock, J. M. Muir and D. W. H. Rankin, *J. Mol. Struct.*, 1990, **220**, 205–215.
34 S. A. Peebles and R. A. Peebles, *J. Mol. Struct.*, 2003, **657**, 107–116.
35 W. Caminati and A. M. Mirri, *Chem. Phys. Lett.*, 1971, **12**, 127–130.
36 O. Dorosh, E. Białkowska-Jaworska, Z. Kisiel and L. Pszczółkowski, *J. Mol. Spectrosc.*, 2007, **246**, 228–232.
37 A. M. Mirri and W. Caminati, *Chem. Phys. Lett.*, 1971, **8**, 409–412.
38 M. Onda, T. Odaka, H. Miyazaki, M. Mori, I. Yamaguchi and Y. Niide, *J. Mol. Spectrosc.*, 1996, **176**, 17–22.
39 M. Onda, T. Odaka, H. Miyazaki, M. Mori, I. Yamaguchi and Y. Niide, *J. Mol. Spectrosc.*, 1994, **165**, 426–432.
40 S. A. Peebles and R. A. Peebles, *J. Mol. Struct.*, 2002, **607**, 19–29.
41 A. Cairncross, W. A. Sheppard and E. Wonchoba, *Org. Synth.*, 2003, **59**, 122.
42 A. Haloui and E. Haloui, *J. Mol. Struct.*, 2014, **1068**, 140–148.
43 A. Haloui and E. Haloui, *Magn. Reson. Chem.*, 2011, **49**, 717–724.
44 M. J. Frisch, G. W. Trucks, H. B. Schlegel, G. E. Scuseria, M. A. Robb, J. R. Cheeseman, G. Scalmani, V. Barone, G. A. Petersson, H. Nakatsuji and others, Gaussian Inc., Wallingford CT.
45 C. Calabrese, A. Maris, I. Uriarte, E. J. Cocinero and S. Melandri, *Chem. – Eur. J.*, 2017, **23**, 3595–3604.
46 M. Reiher, *Wiley Interdiscip. Rev.: Comput. Mol. Sci.*, 2012, **2**, 139–149.
47 T. H. Dunning Jr, *J. Chem. Phys.*, 1989, **90**, 1007–1023.
48 A. K. Wilson, D. E. Woon, K. A. Peterson and T. H. Dunning Jr, *J. Chem. Phys.*, 1999, **110**, 7667–7676.
49 B. P. Pritchard, D. Altarawy, B. Didier, T. D. Gibson and T. L. Windus, *J. Chem. Inf. Model.*, 2019, **59**, 4 814–4820.
50 H. M. Pickett, *J. Mol. Spectrosc.*, 1991, **148**, 371–377.
51 J. K. G. Watson, *Vibrational spectra and structure Vol VI*, Elsevier Science Publishers B.V., Oxford, New York, 1977.
52 J. Kraitchman, *Am. J. Phys.*, 1953, **21**, 17–24.

53 C. C. Costain, *Trans. Am. Crystallogr. Assoc.*, 1966, **2**, 157–164.
54 Z. Kisiel, *J. Mol. Spectrosc.*, 2003, **218**, 58–67.
55 E. A. C. Lucken and E. Schempp, *Phys. Today*, 1969, **23**, 56–57.
56 E. D. Glendening, A. E. Reed, J. E. Carpenter and F. Weinhold, *NBO Version 3.1*, 2003.
57 G. G. Brown, B. C. Dian, K. O. Douglass, S. M. Geyer, S. T. Shipman and B. H. Pate, *Rev. Sci. Instrum.*, 2008, **79**, 53103.
58 J.-U. Grabow, W. Stahl and H. Dreizler, *Rev. Sci. Instrum.*, 1996, **67**, 4072–4084.
59 T. J. Balle and W. H. Flygare, *Rev. Sci. Instrum.*, 1981, **52**, 33–45.
60 W. Caminati, A. Millemaggi, J. L. Alonso, A. Lesarri, J. C. López and S. Mata, *Chem. Phys. Lett.*, 2004, **392**, 1–6.
61 W. Caminati, L. Evangelisti, G. Feng, B. M. Giuliano, Q. Gou, S. Melandri and J.-U. Grabow, *Phys. Chem. Chem. Phys.*, 2016, **18**, 17851–17855.